EUROPEAN ORGANISATION FOR NUCLEAR RESEARCH

CERN-PPE/91-31
20 February 1991

A Model Independent Observation of the String Effect using Quark Tagging at LEP

The OPAL Collaboration

Abstract

Quark and gluon jets in 3-jet events from hadronic Z^0 decays are identified through use of the semi-leptonic decays of charm and bottom quarks. This tagging method allows geometrically symmetric or transposed configurations of the quark and gluon jets to be selected, permitting a study of the asymmetry in the population of particles in the regions between jets, commonly called the string effect, which avoids restrictions present in previous studies. In particular, our demonstration of a population asymmetry is performed without use of a model. Our results imply that dynamical differences exist between quarks and gluons or between quark-antiquark and quark-gluon jet systems with respect to their particle production properties.

(Submitted to Physics Letters B)

The OPAL Collaboration

M.Z. Akrawy[13], G. Alexander[23], J. Allison[16], P.P. Allport[5], K.J. Anderson[9], J.C. Armitage[6], P. Ashton[16], A. Astbury[a], D. Axen[b], G. Azuelos[18,c], J.T.M. Baines[16], A.H. Ball[17], J. Banks[16], G.J. Barker[13], R.J. Barlow[16], J.R. Batley[5], G. Beaudoin[18], A. Beck[23], J. Becker[10], T. Behnke[8], K.W. Bell[20], G. Bella[23], S. Bethke[11], O. Biebel[3], U. Binder[10], I.J. Bloodworth[1], P. Bock[11], S. Bougerolle[b], B.B. Brabson[12], H. Breuker[8], R.M. Brown[20], R. Brun[8], A. Buijs[8], H.J. Burckhart[8], P. Capiluppi[2], R.K. Carnegie[6], A.A. Carter[13], J.R. Carter[5], C.Y. Chang[17], D.G. Charlton[8], J.T.M. Chrin[16], P.E.L. Clarke[25], I. Cohen[23], W.J. Collins[5], J.E. Conboy[15], M. Cooper[22], M. Couch[1], M. Coupland[14], M. Cuffiani[2], S. Dado[22], G.M. Dallavalle[2], S. De Jong[8], P. Debu[21], M.M. Deninno[2], A. Dieckmann[11], M. Dittmar[4], M.S. Dixit[7], E. Duchovni[26], I.P. Duerdoth[16], D.J.P. Dumas[6], P.A. Elcombe[5], P.G. Estabrooks[6], E. Etzion[23], F. Fabbri[2], P. Farthouat[21], M. Fincke-Keeler[a], H.M. Fischer[3], D.G. Fong[17], C. Fukunaga[24], A. Gaidot[21], O. Ganel[26], J.W. Gary[11], J. Gascon[18], N.I. Geddes[20], C. Geich-Gimbel[3], S.W. Gensler[9], F.X. Gentit[21], G. Giacomelli[2], V. Gibson[5], W.R. Gibson[13], J.D. Gillies[20], J. Goldberg[22], M.J. Goodrick[5], W. Gorn[4], E. Gross[26], H. Hagedorn[10], J. Hagemann[8], G.G. Hanson[12], M. Hansroul[8], C.K. Hargrove[7], I. Harrus[22], J. Hart[5], P.M. Hattersley[1], M. Hauschild[8], C.M. Hawkes[8], E. Heflin[4], R.J. Hemingway[6], R.D. Heuer[8], J.C. Hill[5], S.J. Hillier[1], D.A. Hinshaw[18], C. Ho[4], J.D. Hobbs[9], P.R. Hobson[25], D. Hochman[26], B. Holl[8], R.J. Homer[1], S.R. Hou[17], C.P. Howarth[15], R.E. Hughes-Jones[16], R. Humbert[10], P. Igo-Kemenes[11], H. Ihssen[11], D.C. Imrie[25], L. Janissen[6], A. Jawahery[17], P.W. Jeffreys[20], H. Jeremie[18], M. Jimack[8], M. Jobes[1], R.W.L. Jones[13], P. Jovanovic[1], D. Karlen[6], K. Kawagoe[21], T. Kawamoto[24], R.K. Keeler[a], R.G. Kellogg[17], B.W. Kennedy[15], C. Kleinwort[8], D.E. Klem[19], G. Knop[3], T. Kobayashi[24], T.P. Kokott[3], L. Köpke[8], R. Kowalewski[6], H. Kreutzmann[3], J. von Krogh[11], J. Kroll[9], M. Kuwano[24], P. Kyberd[13], G.D. Lafferty[16], F. Lamarche[18], W.J. Larson[4], J.G. Layter[4], P. Le Du[21], P. Leblanc[18], A.M. Lee[17], M.H. Lehto[15], D. Lellouch[8], P. Lennert[11], C. Leroy[18], L. Lessard[18], S. Levegrün[3], L. Levinson[26], S.L. Lloyd[13], F.K. Loebinger[16], J.M. Lorah[17], B. Lorazo[18], M.J. Losty[7], X.C. Lou[12], J. Ludwig[10], M. Mannelli[8], S. Marcellini[2], G. Maringer[3], A.J. Martin[13], J.P. Martin[18], T. Mashimo[24], P. Mättig[3], U. Maur[3], T.J. McMahon[1], J.R. McNutt[25], F. Meijers[8], D. Menszner[11], F.S. Merritt[9], H. Mes[7], A. Michelini[8], R.P. Middleton[20], G. Mikenberg[26], J. Mildenberger[6], D.J. Miller[15], C. Milstene[23], M. Minowa[24], W. Mohr[10], C. Moisan[18], A. Montanari[2], T. Mori[24], M.W. Moss[16], P.G. Murphy[16], W.J. Murray[5], B. Nellen[3], H.H. Nguyen[9], M. Nozaki[24], S.W. O'Neale[8,d], B.P. O'Neill[4], F.G. Oakham[7], F. Odorici[2], M. Ogg[6], H.O. Ogren[12], H. Oh[4], C.J. Oram[c], M.J. Oreglia[9], S. Orito[24], J.P. Pansart[21], P. Paschievici[26], G.N. Patrick[20], S.J. Pawley[16], P. Pfister[10], J.E. Pilcher[9], J.L. Pinfold[26], D.E. Plane[8], P. Poffenberger[a], B. Poli[2], A. Pouladdej[6], E. Prebys[8], T.W. Pritchard[13], H. Przysiezniak[18], G. Quast[8], M.W. Redmond[9], D.L. Rees[1], M. Regimbald[18], K. Riles[4], C.M. Roach[5], S.A. Robins[13], A. Rollnik[3], J.M. Roney[9], S. Rossberg[10], A.M. Rossi[2,f], P. Routenburg[6], K. Runge[10], O. Runolfsson[8], D.R. Rust[12], S. Sanghera[6], M. Sasaki[24], A.D. Schaile[10], O. Schaile[10], W. Schappert[6], P. Scharff-Hansen[8], P. Schenk[a], H. von der Schmitt[11], S. Schreiber[3], J. Schwarz[10], M. Settles[12], B.C. Shen[4], P. Sherwood[15], R. Shypit[b], A. Simon[3], P. Singh[13], G.P. Siroli[2], A. Skuja[17], A.M. Smith[8], T.J. Smith[8], G.A. Snow[17], R. Sobie[g], R.W. Springer[17], M. Sproston[20], K. Stephens[16], H.E. Stier[10], R. Stroehmer[11], D. Strom[9], H. Takeda[24], T. Takeshita[21], P. Taras[18], S. Tarem[26], N.J. Thackray[1], T. Tsukamoto[24], M.F. Turner[5], G. Tysarczyk-Niemeyer[11], D. Van den plas[18], R. Van Kooten[8], G.J. VanDalen[4], G. Vasseur[21], C.J. Virtue[19], A. Wagner[11], C. Wahl[10], J.P. Walker[1], C.P. Ward[5], D.R. Ward[5], P.M. Watkins[1], A.T. Watson[1], N.K. Watson[1], M. Weber[11], S. Weisz[8], P.S. Wells[8], N. Wermes[11], M. Weymann[8], G.W. Wilson[21], J.A. Wilson[1], I. Wingerter[8], V-H. Winterer[10], N.C. Wood[15], S. Wotton[8], T.R. Wyatt[16], R. Yaari[26], Y. Yang[1,h], G. Yekutieli[26], T. Yoshida[24], I. Zacharov[8], W. Zeuner[8], G.T. Zorn[17].

[1]School of Physics and Space Research, University of Birmingham, Birmingham, B15 2TT, UK
[2]Dipartimento di Fisica dell' Università di Bologna and INFN, Bologna, 40126, Italy
[3]Physikalisches Institut, Universität Bonn, D-5300 Bonn 1, FRG
[4]Department of Physics, University of California, Riverside, CA 92521 USA
[5]Cavendish Laboratory, Cambridge, CB3 0HE, UK
[6]Carleton University, Dept of Physics, Colonel By Drive, Ottawa, Ontario K1S 5B6, Canada
[7]Centre for Research in Particle Physics, Carleton University, Ottawa, Ontario K1S 5B6, Canada
[8]CERN, European Organisation for Particle Physics, 1211 Geneva 23, Switzerland
[9]Enrico Fermi Institute and Department of Physics, University of Chicago, Chicago Illinois 60637, USA
[10]Fakultät für Physik, Albert Ludwigs Universität, D-7800 Freiburg, FRG
[11]Physikalisches Institut, Universität Heidelberg, Heidelberg, FRG
[12]Indiana University, Dept of Physics, Swain Hall West 117, Bloomington, Indiana 47405, USA
[13]Queen Mary and Westfield College, University of London, London, E1 4NS, UK
[14]Birkbeck College, London, WC1E 7HV, UK
[15]University College London, London, WC1E 6BT, UK
[16]Department of Physics, Schuster Laboratory, The University, Manchester, M13 9PL, UK
[17]Department of Physics and Astronomy, University of Maryland, College Park, Maryland 20742, USA
[18]Laboratoire de Physique Nucléaire, Université de Montréal, Montréal, Quebec, H3C 3J7, Canada
[19]National Research Council of Canada, Herzberg Institute of Astrophysics, Ottawa, Ontario K1A 0R6, Canada
[20]Rutherford Appleton Laboratory, Chilton, Didcot, Oxfordshire, OX11 0QX, UK
[21]DPhPE, CEN Saclay, F-91191 Gif-sur-Yvette, France
[22]Department of Physics, Technion-Israel Institute of Technology, Haifa 32000, Israel
[23]Department of Physics and Astronomy, Tel Aviv University, Tel Aviv 69978, Israel
[24]International Centre for Elementary Particle Physics and Dept of Physics, University of Tokyo, Tokyo 113, and Kobe University, Kobe 657, Japan
[25]Brunel University, Uxbridge, Middlesex, UB8 3PH UK
[26]Nuclear Physics Department, Weizmann Institute of Science, Rehovot, 76100, Israel
[§]University of British Columbia, Dept of Physics, 6224 Agriculture Road, Vancouver BC V6T 2A6, Canada
[§§]University of Victoria, Dept of Physics, P O Box 1700, Victoria BC V8W 2Y2, Canada

[a]Univ of Victoria, Victoria, Canada
[b]Univ of British Columbia, Vancouver, Canada
[c]and TRIUMF, Vancouver, Canada
[d]On leave from Birmingham University
[e]Univ of Victoria, and TRIUMF, Canada
[f]Present address: Dipartimento di Fisica, Università della Calabria and INFN, 87036 Rende, Italy
[g]Univ of British Columbia and IPP, Canada
[h]On leave from Research Institute for Computer Peripherals, Hangzhou, China

1 Introduction

The string effect in e^+e^- annihilations was first introduced as an experimentally tractable observable to test the mechanism for the transformation of partons into hadrons (fragmentation) [1]. Consider a 3-jet quark-antiquark-gluon ($q\bar{q}g$) event from e^+e^- annihilation as is illustrated in figure 1 (a). In the string fragmentation model of the Lund group [2], a one dimensional confinement field or "string" connects the quark and antiquark with the gluon, as shown by the dotted lines. This leads to an asymmetry by which regions A and B in figure 1 (a) obtain larger relative populations of hadrons than does region C. In contrast, in the independent fragmentation model [3, 4], the fragmentation of each parton is independent from that of all others. There is no dynamical mechanism, except differences in the properties of quark and gluon fragmentation, to generate an asymmetry in the particle populations between the different inter-jet regions. It has been shown [5] that an asymmetry in the particle population between jets in 3-jet events, which is qualitatively similar to that predicted by the Lund model, also arises directly from perturbative Quantum Chromodynamics (QCD): here it is necessary to invoke local parton hadron duality [6] to relate the QCD predictions to the observed hadron spectra. In the case of the perturbative calculations, the asymmetry arises from interference among the soft gluons radiated from the q, $\bar{q}$ and g (coherence). In this paper "string effect" is used to indicate the experimental observation of an asymmetry in the particle population between jets and not to imply a particular interpretation, be it Lund strings, quark-gluon differences, coherence or some other phenomenon.

The string effect was first observed by the JADE Collaboration [7] at $\sqrt{s} = 34$ GeV, who measured a population asymmetry in agreement with the predictions of the Lund model. Similar asymmetries were subsequently observed at $\sqrt{s} \approx 30$ GeV by the TPC/2γ [8], TASSO [9] and MARK2 [10] experiments. For all these studies, the gluon jet was identified by assuming it was the lowest energy jet in the 3-jet event. As a kinematical consequence, the angle between the quark and antiquark jets (ψ_C in figure 1 (a)) was larger (usually much larger) than the angles between the quark and gluon or between the antiquark and gluon jets (ψ_A and ψ_B): thus a geometric asymmetry was present between the different inter-jet regions. To demonstrate that the string effect was not artificially introduced because of this geometric asymmetry, the independent fragmentation model was used or else the $q\bar{q}g$ events were compared to QED radiative $q\bar{q}\gamma$ events with similar event kinematics. It was shown that the independent fragmentation model did not yield a significant asymmetry, even when differences between quark and gluon fragmentation were included, which led to the interpretation that the measured asymmetry was of dynamical origin.

Recently it has been suggested [11] that a new generation of the independent fragmentation model, with a more careful treatment of the transverse structure of jets [12], can reproduce the published experimental data on the string effect including the $q\bar{q}g$ vs. $q\bar{q}\gamma$ comparisons. On this basis, Ballocchi and Odorico [11] have argued that there is no need for a dynamical mechanism to explain the observed population asymmetries, but that they can be explained as being a trivial consequence of the geometric asymmetry between the different inter-jet regions inherent to the energy tagging method.

Here we report an experimental observation of the string effect by the OPAL Collaboration at the CERN e^+e^- collider LEP, which relies on the semi-leptonic decays of charm and bottom

quarks to separate quark and gluon jets in 3-jet events produced in hadronic Z^0 decays. This method makes use of the fact that the principal known source of high momentum leptons in e^+e^- hadronic annihilation events are the weak decays of charm and bottom quarks and that these latter are produced almost in their entirety at the electro-weak vertex: thus the gluon jet in $e^+e^- \rightarrow q\bar{q}g$ events rarely contains a high momentum lepton. The lepton tagging of quark jets allows the selection of events for which the angle between the quark and gluon jets is essentially the same as that between the quark and antiquark jets, corresponding to $\psi_A \approx \psi_C$ in figure 1 (a), or else of events in two different samples which have the same event kinematics, but with the gluon jet direction and energy transposed with those of the quark or antiquark (see figure 1 (b) in comparison to figure 1 (a)). The geometric symmetry in or between these events makes possible a direct comparison of the particle populations in the different inter-jet regions, with no need for the independent fragmentation model or a $q\bar{q}\gamma$ event sample as a reference.

2 The OPAL Detector and Data Selection

The main features of the OPAL detector are presented elsewhere [13]. Here we give a brief overview. The tracking of charged particles is performed with the central tracking detector, which contains a vertex chamber, a jet chamber and a chamber for measurements in the z direction, all enclosed by a solenoidal magnet coil (z is the coordinate parallel to the beam axis). The principal tracking chamber is the jet chamber, which provides up to 159 space points and close to 100% tracking efficiency for charged tracks in the region $|cos\theta| < 0.92$, with θ the polar angle. Energy loss dE/dx measurements from the jet chamber are used for the identification of charged particles. Electromagnetic energy deposits ("clusters") are measured with the electromagnetic calorimeter, a detector of lead-glass blocks located in both the barrel and endcap regions, each block subtending 40x40 mrad^2, for a total detector solid angle coverage of 98% of 4π. Both the barrel and endcap electromagnetic calorimeters are instrumented with a presampler, composed of limited streamer chambers for the barrel and of thin multiwire chambers for the endcap. The hadron calorimeter contains a barrel component ($|cos\theta| < 0.81$) with 9 layers of limited streamer tubes separated by 8 layers of iron slabs, and an endcap component ($0.81 < |cos\theta| < 0.91$) with 8 layers of streamer tubes and 7 layers of iron. The layers are grouped into projective towers which subtend approximately 7.5° in azimuth ϕ and 5° in polar angle. Signals induced on 4 mm wide strips on each hadron calorimeter streamer tube chamber provide precise $r - \phi$ tracking information; r is the coordinate perpendicular to the beam axis. The muon detector contains a barrel component of 4 layers of planar drift chambers in the region $|cos\theta| < 0.68$ and an endcap component of 4 layers of limited streamer chambers in the region $0.60 < |cos\theta| < 0.98$.

The trigger and event selection for hadronic events are described in [14]. Additional selection criteria were applied for this analysis to reduce the small level of background and to obtain well measured tracks and events. Charged tracks were accepted if they originated from within 5 cm of the interaction point in the plane perpendicular to the beam axis. The minimum transverse momentum was set at 150 MeV/c, the angle relative to the beam direction had to exceed 20° and the track was required to have at least 40 measured space points. Electromagnetic clusters were accepted if they had at least 100 or 300 MeV of energy, depending on whether they appeared in the barrel or endcap. Each electromagnetic cluster was required to be spread over at least

2 lead-glass blocks. Only those clusters not associated with a charged track were included. A cluster in the barrel calorimeter was associated with a charged track if the extrapolated track coordinates at the entrance of the calorimeter matched to better than 60 mrad in polar angle θ and to better than 80 mrad in azimuthal angle ϕ with the cluster position. For the endcap calorimeter the matching criterion was 50 mrad for both θ and ϕ. Hadronic events accepted for this analysis had at least 5 charged tracks and a direction for the thrust axis, defined using the accepted charged tracks and electromagnetic clusters, which was at least 30^o away from the beam axis. Starting with an event sample of 140,189 multi-hadron events corresponding to a luminosity of about 6.5 pb^{-1}, we obtained 116,953 events at c.m. energies between 88.3 and 95.0 GeV after these cuts. The mean c.m. energy value for the events is 91.3 GeV.

3 3-jet Event Selection

To select 3-jet events, we employ an invariant mass algorithm based on a modified version of the JADE jet-finder [15]. In this letter, particles are defined to be charged tracks and unassociated clusters which satisfy the criteria of section 2. Beginning with the assumption that all particles in an event form a separate jet, the 2 jets with the smallest scaled pair mass $y_{ij} = M_{ij}^2/E_{vis.}^2$ are combined into a single jet if y_{ij} is below a threshold value y_{cut}. Here $E_{vis.}$ is the sum over the energies of the particles in the event. The combined jet is given an energy equal to the magnitude of its 3-momentum. This recombination scheme, the so called "P scheme" [16], yields better resolutions for the final jet directions and energies, in the sense described below, than do other available schemes. This process is continued until all jet pairs satisfy the resolution criterion $y_{ij} > y_{cut}$. For our analysis we choose the resolution value $y_{cut} = 0.03$, corresponding to an average jet mass of about 12 GeV: this is sufficiently above the b quark mass value that most decay products from heavy quark hadrons remain in the same jet while being small enough to remain efficient for selecting events with prominent 3 jet structure.

Those events with exactly 3 reconstructed jets are retained for further analysis. Each particle in an event is associated with one of the 3 jets by the jet-finding algorithm. The sum of the angles between the 3 jets is required to exceed 358^o to eliminate non-planar events. Each of the 3 jets must contain at least 3 particles, have a visible energy larger than 5 GeV and a polar angle with respect to the beam axis of at least 30^o. The jets are assigned a calculated energy based on the angles between the jets, assuming massless kinematics.[1] The calculated jet energy is required to be larger than 5 GeV while the fractional difference between the calculated and visible jet energy must satisfy

$$\left| \frac{E_{jet}^{calculated} - c \cdot E_{jet}^{visible}}{E_{jet}^{calculated}} \right| < 0.4 \qquad (1)$$

for each jet, where the multiplicative factor c corrects the visible energy of a jet for the difference between the mean values of the calculated and visible jet energy distributions; c has a value of 1.16, 1.33 and 1.23 for the jet with the highest, the central and the lowest visible energy value. This last cut eliminates events for which there is a large difference between the calculated and

[1] If jet α is opposite region α in figure 1 (a), with $\alpha = A$, B or C, then its energy E_α is $E_\alpha = E_{c.m.} \cdot sin\psi_\alpha/(sin\psi_A + sin\psi_B + sin\psi_C)$.

visible energies of a jet, which we assume to be due to imperfect jet reconstruction. In total we obtain 22,721 3-jet events after applying these criteria.

The jet energy and angular resolution values are a measure of the quality of the jet reconstruction. Our experimental demonstration of the string effect, presented in section 5, does not employ a model, but we use the Jetset parton shower model [17], version 7.2, after processing through the OPAL detector simulation program [18], to estimate these resolution values for informational purposes. This model, with its principal parameters adjusted to describe global event shape measurements by OPAL [19], provides a good description of the relevant experimental distributions after being subjected to the same reconstruction, selection and analysis procedures as the data. Those simulated events which satisfy the 3-jet event criteria given above are examined at the parton level: the P-scheme jet-finder with $y_{cut} = 0.03$ is applied to the underlying parton states. About 10% of the events do not have 3 jets at the parton level for $y_{cut} = 0.03$; most of these events ($\approx 80\%$) fall just outside the 3-jet class at the parton level and enter that class for y_{cut} values in the range from 0.02 to 0.04. For the 10% of the events, we therefore apply the jet-finder at the parton level such that exactly 3 jets are always found. The 3 parton jets in the Monte Carlo events are associated with the 3 hadron jets by finding the combination which minimizes the sum of the angular differences between them. The jet energy resolution is taken to be the difference between the energy of a parton jet and the calculated energy of its associated hadron jet, normalized by the former, and has a RMS value of 8.1%, 11.4% and 22.1% for the hadron jet with the highest, the central and the lowest calculated energy value, respectively. The angular resolution values are the RMS differences between the hadron and associated parton jet directions and are 2.6°, 3.9° and 10.6°, respectively. The difference between the mean values of the calculated hadron jet energies and the energies of the associated parton jets is about 5% or less in all cases.

4 Semi-leptonic Jet Tagging

Muon candidates are identified within the 3-jet event sample by associating tracks reconstructed in the central tracking detector with track segments reconstructed independently in the hadron calorimeter strips and muon detectors. The muon identification is performed in the polar angle region $|cos\theta| < 0.9$. More details are given in [20].

Electron candidates in the multi-hadron events are identified by requiring that a track reconstructed in the central tracking detector be associated with energy clusters in the presampler and electromagnetic calorimeter. The electron identification is restricted to the range $|cos\theta| < 0.7$. A charged track is associated with a presampler cluster for the purposes of electron identification if its extrapolated coordinates at the entrance of the presampler match to better than 40 mrad in polar angle θ and 60 mrad in azimuthal angle ϕ with the cluster coordinates; the corresponding matching criteria for the calorimeter are 60 and 20 mrad. The energy deposit in the associated presampler cluster is required to be at least 1.25 times larger than that expected for a non-showering relativistic particle. The associated electromagnetic calorimeter cluster must be spread over at least 2 lead-glass blocks, with 90% of the cluster energy contained in either 2 or 3 blocks. The value of energy loss, dE/dx, measured in the jet chamber for the track is required to be consistent with the electron hypothesis (9 to 12 keV/cm), while the (E/p) ratio, which is the energy of the associated electromagnetic calorimeter cluster divided

by the momentum value from the tracking chambers for the electron candidate, must satisfy $0.8 < (E/p) < 1.2$. A secondary vertex reconstruction algorithm is applied to remove e^+e^- pairs arising from photon conversions.

For the subsequent analysis we employ events from the 3-jet sample for which there is a muon candidate with momentum p larger than 3.0 GeV or an electron candidate with p larger than 2.0 GeV. We study two distinct event samples for which quark and gluon jets can be separated with high efficiency, using the lepton tags. For the first sample, a single lepton candidate is required to be present and it must be in one of the two jets with lower energy. The association of a lepton with a jet is taken from its jet-finder assignment. For this "single-tag" sample, the highest energy jet is assumed to be a quark or antiquark jet: this is justified because the gluon jet rarely has the highest energy in $e^+e^- \to q\bar{q}g$ events. The jet with the lepton candidate is the other "quark-tagged" jet; the remaining jet is the "gluon-tagged" jet. In this letter we often refer to the antiquark jet as a "quark jet" since there is no discrimination between quarks and antiquarks in our analysis. The energy difference between the highest energy and gluon-tagged jets is required to exceed 8 GeV to remove the ambiguous region (if the two jets without a lepton are close in energy, there is little information on which is the quark and which is the gluon jet). In total we obtain 1,311 events for this single tag sample: 933 with a muon and 378 with an electron tag. For the second sample, a lepton is required to be present in two of the three jets. The two jets with leptons are the quark-tagged jets; the jet without the lepton is the gluon-tagged jet. Thus the gluon jet is sometimes the highest energy jet in the events of this sample. In total there are 258 events in the double tag sample: 123 with a double muon tag, 30 with a double electron tag and 105 with one muon and one electron. Table 1 summarizes the event selection efficiencies for the single- and double-tag samples.

For informational purposes we again use Jetset, with simulation of the detector and the experimental selection criteria including the lepton tagging, to estimate for the single lepton tag sample that the higher and lower energy quark-tagged jets are correctly identified as being the quark or antiquark jets in $96 \pm 1\%$ and $88 \pm 1\%$ of the events, respectively, where the errors are statistical. The corresponding purity for the gluon-tagged jets is $84 \pm 1\%$. For this study, parton level jets are associated with hadron level jets using the algorithm described in section 3. The gluon jet is the jet which does not contain the primary quark or antiquark from the electro-weak vertex (there is a small background of 0.7% of the events for which the primary quark and antiquark are assigned to the same parton jet). An analogous study for the double tag sample yields the estimate that the quark-tagged jets have purities of $96 \pm 1\%$ and $87 \pm 2\%$, where the first value is for the quark-tagged jet with higher energy, while the gluon-tagged jet has a purity of $84 \pm 2\%$. The main source of background is estimated to be hadronic contamination, that is, charged hadrons which are misidentified as leptons or else leptons from the decays of light-quark hadrons [20]. The purities of the quark and gluon jets are about the same for the single and double tag samples since, having identified the higher energy quark-tagged jet correctly as a quark jet with close to 100% accuracy in both cases, the probability for hadronic contamination in the lower energy quark-tagged jet is similar. The same Monte Carlo events are used to estimate that the flavor composition of the events in the single tag sample is about 47% bottom, 20% charm, 12% strange, 9% up and 12% down. The corresponding estimate for the double tag sample is 70% bottom, 21% charm and 3% each for strange, up and down. The large proportion of bottom and charm quark events, which is due to the lepton tagging of the quark and antiquark jets, is not expected to bias our study of the particle populations between jets as will be discussed in section 6. For the remainder of this

letter we refer to the quark-tagged and gluon-tagged jets as simply the quark (or antiquark) and gluon jets, respectively.

5 The String Effect at 91 GeV

5.1 Symmetrical Quark-Gluon Jet Configurations

To study the string effect we begin with configurations for which the gluon and lower energy quark jets are geometrically symmetric with respect to each other within an event. We thus select events from both the single and double tag samples for which the angle between the gluon and highest energy quark jet is approximately the same as that between the two quark jets, corresponding to the condition $\psi_A \approx \psi_C$ in figure 1 (a). The 3 jets and particle momenta in an event are projected into the event plane, defined by the 2 eigenvectors of the sphericity tensor [21] associated with the 2 largest sphericity eigenvalues. This projection represents only a small correction for the jets since they have been required to be almost co-planar by the 3-jet selection criteria. The azimuthal angles ψ_A and ψ_C between the jets in the event plane are then examined. Events are selected in two configurations: (I) $\psi_A = 150 \pm 10^o$, $\psi_C = 150 \pm 10^o$ and (II) $\psi_A = 130 \pm 10^o$, $\psi_C = 130 \pm 10^o$. In total we obtain 188 events for configuration (I) and 36 events for configuration (II) with the single and double tag samples combined. The number of events, mean jet energies, mean angles between jets and estimated quark and gluon jet purities for these two samples are given in table 2. The purities have been estimated in the manner described in section 4. Other ranges of ψ_A and ψ_C than those of configurations (I) and (II), with symmetry within an event under transposition of the gluon and lower energy quark jet energies and directions, do not contain significant event statistics and are not included in our study.

The inclusive angular distribution of particles or "particle flow," $(1/N)\, dn/d\psi$, is presented in figure 2 for the events of configurations (I) and (II): ψ is the angle in the event plane between a particle and the highest energy quark jet; N is the number of events in the configuration; dn is the number of particles in a bin of width $d\psi$. The distributions of figure 2 are at the detector level, that is, no corrections have been applied to the data. The points with errors in figure 2 show the measured particle flow starting at the higher energy quark jet axis ($\psi \equiv 0^o$), then proceeding through the lower energy quark jet axis ($\psi \approx 150^o$ for figure 2 (a) and $\psi \approx 130^o$ for figure 2 (b)) to the gluon jet ($\psi \approx 210^o$ and $\psi \approx 230^o$), back to the higher energy quark jet ($\psi \equiv 360^o$). The histograms show the particle flow for the same data events, again starting at the higher energy quark axis ($\psi \equiv 0^o$) but this time proceeding in the opposite sense: first through the gluon jet ($\psi \approx 150^o$ and $\psi \approx 130^o$) then through the lower energy quark jet ($\psi \approx 210^o$ and $\psi \approx 230^o$). The distributions shown by the points with errors for $0^o < \psi < 180^o$ are therefore the same as those shown by the histograms for $360^o > \psi > 180^o$, and *vice versa*. The errors are statistical only.

The events in figure 2 are kinematically and geometrically symmetric under transposition of the gluon and lower energy quark jets. Nonetheless a significantly larger population of particles is present in the region between the gluon and higher energy quark jets than in the region between the two quark jets, for both samples. This is illustrated by the excess in the histograms

relative to the points with errors for $\psi \approx 80^o$ in figure 2 (a) and $\psi \approx 70^o$ in figure 2 (b). This asymmetry constitutes direct experimental evidence for the string effect at $\sqrt{s} = 91$ GeV. As a quantitative measure of its statistical significance, we integrate $(1/N)\, dn/d\psi$ over the region $37.5^o < \psi < 112.5^o$ for figure 2 (a) and $32.5^o < \psi < 97.5^o$ for figure 2 (b) and calculate the ratio R of this integral from the quark-gluon to that from the quark-antiquark sectors. These intervals in ψ are chosen because they correspond to the regions from 25% to 75% of the distance between the jet peaks and may be assumed to define the inter-jet regions. We find $R = 1.40 \pm 0.12$ for configuration (I) and $R = 2.46 \pm 0.44$ for configuration (II): the statistical significance of the deviation from unity is thus 3.3 standard deviations (s.d.) in both cases. Table 3 summarizes the values of R. The values of R calculated for charged particles alone and for "energy flow" are also given. The energy flow $(1/E)\, dE/d\psi$ is defined like the particle flow, using charged particles and unassociated calorimeter clusters, except that each particle entry is weighted by its energy value and the normalization is such that the integral of the distribution is one.

We have checked that our asymmetry measurements are unlikely to be biased by the lepton identification criteria by repeating our analysis with the additional requirement that a charged track with momentum $p > 3$ GeV/c be present in the gluon jet. We find consistent results for the asymmetries.

5.2 Transposed Quark-Gluon Jet Configurations

We next extend the study of section 5.1 to event configurations for which transposition of the gluon and lower energy quark jet directions and energies is not symmetric within an event, but for which such transposition yields a different sample of events which is also present in our data at a statistically relevant level (see figure 1 (b) in comparison to figure 1 (a)). In one configuration, events for which $\psi_A = 150 \pm 10^o$ and $\psi_C = 130 \pm 10^o$ in figure 1 (a) are compared to events for which $\psi_A = 130 \pm 10^o$ and $\psi_C = 150 \pm 10^o$. The first of these samples contains 34 events and is designated configuration (IIIa); the second contains 169 events and is designated configuration (IIIb). In the other configuration, the corresponding angles are 170 ± 10^o and 150 ± 10^o, yielding event classes (IVa) and (IVb) with 55 and 210 events, respectively. Note that in configurations (IIIa) and (IVa) the gluon jet has considerably higher energy than the lower energy quark jet, as summarized in table 2. Such configurations are disfavored compared to (IIIb) and (IVb) by the bremsstrahlung spectrum and this accounts for the smaller statistics and lower purity in configurations (IIIa) and (IVa).

Figure 3 shows $(1/N)\, dn/d\psi$, defined as in section 5.1, for configurations (III) and (IV). The distributions are at the detector level, as before. The points with errors in figure 3 (a) show the measured particle flow for configuration (IIIa). The distribution starts at the highest energy quark jet ($\psi \equiv 0^o$), proceeds first through the lower energy quark jet ($\psi \approx 130^o$), then through the gluon jet ($\psi \approx 210^o$). The histogram shows the measured particle flow for configuration (IIIb): here the distribution proceeds first through the gluon jet ($\psi \approx 130^o$), then through the lower energy quark jet ($\psi \approx 210^o$). The distributions in figure 3 (b) are plotted in the same way for classes (IVa) and (IVb). In contrast to the distributions of figure 2, the data points and histograms in figure 3 are constructed from different data samples and so are independent of each other over the entire ψ range: thus independent tests of the string effect can be performed

for both the small ($\psi < 180^o$) and large ($\psi > 180^o$) angle regions.

It is seen in the small angle regions, $\psi < 130^o$ in figure 3 (a) and $\psi < 150^o$ in figure 3 (b), that the particle populations between the quark and antiquark jets (points with errors) are lower than those between the gluon and higher energy quark jets (histograms): this is especially significant for figure 3 (a). These asymmetries are analogous to those observed in section 5.1 for configurations (I) and (II) and constitute independent evidence for the string effect. The significance of the asymmetries can be measured by the ratio R introduced in section 5.1, calculated for $32.5^o < \psi < 97.5^o$ for configuration (III) and for $37.5^o < \psi < 112.5^o$ for configuration (IV): $R = 1.86 \pm 0.29$ and $R = 1.22 \pm 0.15$, respectively, for a statistical deviation from unity of 3.0 and 1.5 s.d.

It is also seen in the large angle regions, $\psi > 210^o$ for figure 3 (a) and $\psi > 190^o$ for figure 3 (b), that the particle population between the quark and antiquark jets (histogram) is lower than that between the gluon and higher energy quark jets (points with errors), which is yet further independent evidence for the string effect. For these last two regions we calculate the ratio R between 247.5^o and 322.5^o for configuration (III) and 232.5^o and 317.5^o for configuration (IV): $R = 1.56 \pm 0.21$ and $R = 1.53 \pm 0.21$, respectively, implying a statistical significance of 2.7 and 2.5 s.d. deviation from unity.

5.3 Combined Asymmetry Ratio $\tilde{R}$

We now combine the signals from the 6 independent regions labeled (1)-(6) in figures 2 and 3 so as to minimize the statistical error. Comparing the values of R for these regions, given in table 3, it is seen that all exhibit a positive asymmetry $R > 1$. The differences in the values of R between the 6 regions can in part be attributed to the kinematical differences between the configurations and in part to the different levels of purity for the quark and gluon jet identification.

To combine the measurements, we re-calculate the particle flow $(1/N)\, dn/d\psi$ for the 6 regions using the normalized angular variable $\tilde{\psi}$, where $\tilde{\psi} = \psi/\psi_A$ for particles between the gluon and higher energy quark jets and $\tilde{\psi} = \psi/\psi_C$ for particles between the quark and antiquark jets (see figure 1 (a)). Thus $0 < \tilde{\psi} < 1$: $\tilde{\psi} \equiv 0$ corresponds to the higher energy quark jet peak while $\tilde{\psi} \equiv 1$ either corresponds to the gluon jet peak or to the lower energy quark jet peak depending on whether it is a quark-gluon or quark-antiquark sector being considered. The combined asymmetry ratio $\tilde{R}$ is:

$$\tilde{R} = \frac{\sum\limits_{region\, i=(1)}^{(6)} \left[\int_{0.25}^{0.75} \left(dn/d\tilde{\psi}\right) d\tilde{\psi}\right]_i^{q\bar{q}}}{\sum\limits_{region\, i=(1)}^{(6)} \left[\int_{0.25}^{0.75} \left(dn/d\tilde{\psi}\right) d\tilde{\psi}\right]_i^{q\bar{q}}} \qquad (2)$$

where the numerator is calculated using the quark-gluon sectors and the denominator using the quark-antiquark sectors. In table 4 we present the measured value of $\tilde{R}$: we find $\tilde{R} = 1.62 \pm 0.07$ which differs from unity by 8.9 s.d. In table 4 the combined ratio value $\tilde{R}$ for charged particles alone and for energy flow are also given.

6 Comparison with Models

Having established the existence of the string effect in our data without use of a model, it is interesting to see how well a QCD model can reproduce the measured asymmetry. The prediction of the Jetset72 [17] parton shower model for the combined asymmetry ratio $\tilde{R}$, calculated after combination of the 6 independent regions (1)-(6) as in section 5.3, is presented in table 4 in comparison to the data. Jetset includes a detailed simulation of soft gluon radiation and interference, Lund string fragmentation and particle decays. The Monte Carlo events have been processed through the OPAL detector simulation program and have been subjected to the same reconstruction and selection procedures as the data, including the separation of quark and gluon jets by lepton tagging. It is seen from table 4 that Jetset predicts a significant string effect asymmetry which is in good agreement with the experimental value.

It is also interesting to examine the predictions of QCD models at the event generator level, that is without experimental cuts and effects of the detector. For this study we include Jetset and the Cojets Monte Carlo, version 6.12 [4]. Cojets differs from Jetset in that it is based on an incoherent parton shower and independent fragmentation. The fragmentation of a gluon is the same as that of a d, u or s quark chosen randomly.[2] Therefore Cojets lacks a dynamical mechanism – either interference effects in the perturbative phase (coherence), string fragmentation or differences between quark and gluon fragmentation properties – to produce a string effect asymmetry. Nonetheless Cojets has been shown to reproduce experimental measurements of the string effect which are based on energy ordering for identification of the gluon jets. The main feature of Cojets which permits this is a mechanism to suppress soft hadrons having large angles with respect to the jet axes [11]: it is this feature which distinguishes Cojets from previous independent fragmentation models. The parameter values we use have been provided by the author of Cojets [22] and yield a good description of global event shape distributions in hadronic Z^0 decays.

Table 5 gives the generator level value of $\tilde{R}$ from Jetset and Cojets. The Monte Carlo events for this table have been subjected to the 3-jet selection criteria given in section 3. We do not apply lepton tagging to separate quark and gluon jets: instead, the gluon jet is identified as the jet without the initial quark or antiquark from the electro-weak vertex, using the technique outlined in section 4. For Jetset we obtain $\tilde{R} = 1.54 \pm 0.02$; Cojets yields $\tilde{R} = 1.02 \pm 0.01$ and thus does not exhibit a significant asymmetry.

To test further the prediction of Cojets, we changed the values of the parameters which control the suppression of soft hadrons having large angles with respect to the jet axes [22]. We purposely chose values for these parameters so that Cojets reached the limit of compatibility with our global event shape data, so that we were sure, in this sense, that we were testing an extreme limit for this mechanism.[3] The asymmetry ratio $\tilde{R}$ derived from Cojets with this changed parameter set is $\tilde{R} = 1.03 \pm 0.01$, which is not much different from that obtained with the default parameters. We also tested an even more extreme change in parameter values [4], as given in table 5, and observed that the prediction of Cojets for $\tilde{R}$ remained essentially stable.

[2] As an option of Cojets, gluon fragmentation can be made different from quark fragmentation.

[3] We changed FRALOG(6) and FRALOQ(6) from their default value of 0.0 to the value 1.0, with the other parameters left unchanged: the χ^2 value derived from 50,000 Monte Carlo events changed from 129 to 571 in comparison to the 110 bins of experimental data presented in [19].

[4] FRALOG(6)=2 and FRALOQ(6)=2; this yields $\chi^2 = 1,358$ for the 110 bins of data in [19].

This implies that suppression of large angle particle production, in the context of independent fragmentation, is unlikely to be an adequate mechanism to describe the population asymmetries for our special geometric configurations. It is possible that Cojets would describe our data if differences in the dynamics of quark and gluon fragmentation were allowed, however. We also tested the independent fragmentation models contained in Jetset [17], for a wide variety of parameter values and options for the perturbative and fragmentation phases. We were unable to obtain a value of $\tilde{R}$ which differed substantially from unity. We thus conclude that our data provide evidence for a dynamical origin for the measured asymmetries, related to the different color charges of quarks and gluons.

The QCD models provide a convenient means to study whether the population asymmetries depend on the quark flavor produced at the electro-weak vertex and thus whether our results are affected by the large proportion of bottom and charm quark events in our data sample. Table 6 gives the value of the asymmetry ratio R calculated from Jetset for samples of events for which the parton showers are initiated either by $d\bar{d}$ or $b\bar{b}$ pairs, for the 6 independent regions used for our string effect measurements (cf. table 3). For this study, full simulation of the detector has been included. Our standard 3-jet event selection has been applied except the gluon jets have been identified "perfectly" using the Monte Carlo information, as for the samples of table 5. It is seen that the $d\bar{d}$ events yield the same asymmetry values R as the $b\bar{b}$ events within the statistical errors, from which we conclude that our results are not strongly affected by the mixture of quark flavors, e.g. by such considerations as the properties of b quark fragmentation or B hadron decay.[5]

7 Discussion and Summary

An experimental observation of the asymmetry in particle population between different inter-jet regions in e^+e^- 3-jet events, or the string effect, has been presented for $\sqrt{s} \approx 91$ GeV. The quark and gluon jets in the 3-jet samples have been separated through observation of the semi-leptonic decays of heavy (c and b) quarks. This lepton tagging method allows the selection of a gluon jet whose energy is the same or larger than that of a quark jet in the same event, in contrast to previous studies of the string effect where energy ordering was used to separate quark and gluon jets. The energy ordering results in a geometric asymmetry between the different inter-jet regions which considerably complicates the interpretation of the asymmetries, a restriction not present for our analysis. In contrast to these previous studies, our analysis does not require a model or QED radiative $q\bar{q}\gamma$ event sample as a reference. Use of leptons from heavy quark decays has long been advocated as a means to separate quark and gluon jets in e^+e^- annihilation 3 jet events (see for example [5]): to our knowledge our study is the first experimental analysis to employ this technique. In addition, we have introduced the idea of using 3-jet events for which a symmetry exists under interchange of the gluon jet energy and direction with those of a quark jet. Such a technique could also be applied to the direct study of quark-gluon jet differences.

From a total of 1,569 3-jet events with a single or double lepton tag and for which the

[5] In perturbative QCD there is also no difference expected for the population asymmetries between jets in light and heavy quark events, for the angular configurations selected for our analysis, see [23].

event-by-event separation of the quark and gluon jets is possible with a high ($\approx 80\%$) reliability, we have selected 692 events from four special geometric classes whose symmetry permits a simple and direct comparison of the different inter-jet particle densities. We perform 6 independent comparisons of the particle population between a quark and gluon jet relative to that between a quark and antiquark jet which have the same energies and which are embedded into a geometrically almost-identical event configuration. In all 6 cases we observe that the particle density between the quark and gluon jets is larger than that between the quark and antiquark jets: when the 6 signals are combined this leads to an asymmetry which differs from unity by 8.9 s.d. Because of the symmetry of the events in our study, it is difficult to see how an independent fragmentation model based on identical fragmentation properties for quarks and gluons could explain our data. We have verified that the independent fragmentation model of Odorico, which has been shown to reproduce the qualitative features of previous string effect measurements, does not predict an asymmetry for our special geometric event classes, even for an extreme set of parameter values to suppress large angle soft particle production (if equal properties for quark and gluon fragmentation are assumed). Our asymmetry measurements imply that dynamical differences exist between quarks and gluons or between quark-gluon and quark-antiquark systems (or both) with regard to their particle production properties. These differences could be explained by coherence in perturbative QCD (assuming local parton hadron duality), string models for fragmentation or possibly by differences between quark and gluon jet fragmentation.

8 Acknowledgements

We thank V. Khoze for commenting on the text. It is a pleasure to thank the SL Division for the efficient operation of the LEP accelerator and their continuing close cooperation with our experimental group. In addition to the support staff at our own institutions we are pleased to acknowledge the following :

Department of Energy, USA
National Science Foundation, USA
Science and Engineering Research Council, UK
Natural Sciences and Engineering Research Council,Canada
Israeli Ministry of Science
Minerva Gesellschaft
The Japanese Ministry of Education, Science and Culture (the Monbusho) and a grant under the Monbusho International Science Research Program.
American Israeli Bi-national Science Foundation.
Direction des Sciences de la Matière du Commissariat à l'Energie Atomique, France.
The Bundesministerium für Forschung und Technologie, FRG.
and The A.P. Sloan Foundation.

References

[1] B. Andersson, G. Gustafson, T. Sjöstrand, Phys. Lett. **B94** (1980) 211.

[2] B. Andersson *et al.*, Phys. Rep. **97** (1983) 31.

[3] R. Field and R.P. Feynman, Nucl. Phys. **B136** (1978) 1;
P. Hoyer *et al.*, Nucl. Phys. **B161** (1979) 349;
A. Ali *et al.*, Phys. Lett. **B93** (1980) 155.

[4] R. Odorico, Comp. Phys. Comm. **32** (1984) 139; Comp. Phys. Comm. **59** (1990) 527.

[5] Ya.I. Azimov *et al.*, Phys. Lett. **B165** (1985) 147.

[6] D. Amati and G. Veneziano, Phys. Lett. **B83** (1979) 87;
Ya.I. Azimov *et al.*, Z. Phys. **C27** (1985) 65.

[7] JADE Collaboration, W. Bartel *et al.*, Phys. Lett. **B101** (1981) 129;
Z. Phys. **C21** (1983) 37.

[8] TPC/2γ Collaboration, H. Aihara *et al.*, Phys. Rev. Lett. **54** (1985) 270;
Z. Phys. **C28** (1985) 31; Phys. Rev. Lett. **57** (1986) 945.

[9] TASSO Collaboration, M. Althoff *et al.*, Z. Phys. **C29** (1985) 29.

[10] MARK2 Collaboration, P. D. Sheldon *et al.* Phys. Rev. Lett. **57** (1986) 1398.

[11] G. Ballocchi and R. Odorico, Nucl. Phys. **B345** (1990) 173.

[12] P. Biddulph and G. Thompson, Comp. Phys. Comm. **54** (1989) 13.

[13] OPAL Collaboration, K. Ahmet *et al.*, CERN-PPE/90-114 (1990), submitted to Nucl. Instr. and Meth.

[14] OPAL Collaboration, M. Z. Akrawy *et al.*, Phys. Lett. **B231** (1989) 530;
Phys. Lett. **B235** (1990) 379.

[15] JADE Collaboration, W. Bartel *et al.*, Z. Phys. **C33** (1986) 23;
OPAL Collaboration, M. Z. Akrawy *et al.*, CERN-PPE/90-143.

[16] Z. Kunszt and P. Nason, Z. Physics at LEP 1 vol.1, CERN-89-08, eds. G. Altarelli, R. Kleiss and G. Verzegnassi, Geneva (1989).

[17] T. Sjöstrand, Comp. Phys. Comm. **39** (1986) 347;
T. Sjöstrand and M. Bengtsson, Comp. Phys. Comm. **43** (1987) 367.

[18] J. Allison *et al.*, Comp. Phys. Comm. **47** (1987) 55.

[19] OPAL Collaboration, M. Z. Akrawy *et al.*, Z. Phys. **C47** (1990) 505.

[20] OPAL Collaboration, M. Z. Akrawy *et al.*, to be published.

[21] J. D. Bjorken and S. J. Brodsky, Phys. Rev. **D1** (1970) 1416;
MARK2 Collaboration, G. Hanson *et al.*, Phys. Rev. **D26** (1982) 991.

[22] R. Odorico, private communication.

[23] V. A. Khoze, Proc. Int. Symp. on Lepton Photon Interactions, Stanford, 1989 (World Scientific).

Table 1: Summary of event selection efficiences. For the double tag sample, the first particle type in the hyphenated expressions refers to the lepton-tagged jet with the higher energy.

Total Nr. of multi-hadron events	140,189
Nr. after containment cuts	116,953
Nr. of 3-jet events	22,721
Nr. of 3-jet events with 1 lepton	2,992
lepton not in highest energy jet	1,471
8 GeV jet energy difference cut	1,311
Nr. of 3-jet events with 2 leptons	258
Single Tag sample:	
Total Nr. events	1,311
muon tags	933
electron tags	378
Double Tag sample:	
Total Nr. events	258
muon-muon tags	123
muon-electron tags	56
electron-muon tags	49
electron-electron tags	30

Table 2: Event statistics, mean angles between jets, mean calculated jet energies and estimated quark and gluon jet purities (with statistical errors) for the 6 data samples in our study; $q1$ and $q2$ refer to the quark or antiquark jet with higher and lower energy, respectively.

Event sample	Nr. events	$< \psi_A >$ (deg.)	$< \psi_C >$ (deg.)	$< E_{q_1} >$ (GeV)	$< E_{q_2} >$ (GeV)	$< E_g >$ (GeV)	P_{q_1} (%)	P_{q_2} (%)	P_g (%)
(I)	188	150.7	152.0	42.6	24.9	23.9	98 ± 1	81 ± 3	78 ± 3
(II)	36	132.1	135.4	37.4	27.7	26.4	83 ± 6	85 ± 5	70 ± 7
(IIIa)	34	150.2	133.6	40.5	20.8	30.3	97 ± 2	71 ± 5	68 ± 6
(IIIb)	169	129.9	152.3	40.2	31.8	19.2	95 ± 1	90 ± 2	87 ± 2
(IVa)	55	164.6	149.8	43.8	16.8	30.7	98 ± 2	51 ± 7	49 ± 7
(IVb)	210	148.1	165.5	43.8	32.0	15.5	99 ± 1	86 ± 2	86 ± 2

Table 3: Values of the asymmetry ratio R for the 6 independent regions (1)-(6) in our study. The deviation of R from unity is given in units of standard deviation (σ). The errors are statistical only.

(1) Configuration (I) ($37.5^o < \psi < 112.5^o$)		
All particles	1.40 ± 0.12	$(3.3\ \sigma)$
Charged only	1.50 ± 0.16	$(3.1\ \sigma)$
Energy flow	1.30 ± 0.14	$(2.1\ \sigma)$
(2) Configuration (II) ($32.5^o < \psi < 97.5^o$)		
All particles	2.46 ± 0.44	$(3.3\ \sigma)$
Charged only	2.42 ± 0.59	$(2.4\ \sigma)$
Energy flow	2.56 ± 0.58	$(2.7\ \sigma)$
(3) Configuration (III) ($32.5^o < \psi < 97.5^o$)		
All particles	1.86 ± 0.29	$(3.0\ \sigma)$
Charged only	2.05 ± 0.43	$(2.4\ \sigma)$
Energy flow	1.64 ± 0.32	$(2.0\ \sigma)$
(4) Configuration (III) ($247.5^o < \psi < 322.5^o$)		
All particles	1.56 ± 0.21	$(2.7\ \sigma)$
Charged only	1.71 ± 0.28	$(2.5\ \sigma)$
Energy flow	1.47 ± 0.25	$(1.9\ \sigma)$
(5) Configuration (IV) ($37.5^o < \psi < 112.5^o$)		
All particles	1.22 ± 0.15	$(1.5\ \sigma)$
Charged only	1.21 ± 0.18	$(1.2\ \sigma)$
Energy flow	1.25 ± 0.19	$(1.3\ \sigma)$
(6) Configuration (IV) ($232.5^o < \psi < 317.5^o$)		
All particles	1.53 ± 0.21	$(2.5\ \sigma)$
Charged only	1.62 ± 0.28	$(2.2\ \sigma)$
Energy flow	1.44 ± 0.23	$(1.9\ \sigma)$

Table 4: Values of the combined asymmetry ratio $\tilde{R}$ for data and Monte Carlo. The Monte Carlo values include simulation of the detector and the same analysis procedures as the data. The errors are statistical only.

	All particles	Charged Only	Energy flow
Data	1.62 ± 0.07 $(8.9\ \sigma)$	1.66 ± 0.09 $(7.3\ \sigma)$	1.68 ± 0.09 $(7.6\ \sigma)$
Jetset72	1.67 ± 0.07	1.65 ± 0.08	1.78 ± 0.09

Table 5: Values of the combined asymmetry ratio $\tilde{R}$ for Monte Carlo samples at the event generator level, with perfect gluon jet identification. The errors are statistical only.

Jetset72	1.54 ± 0.02
Cojets612	1.02 ± 0.01
Cojets612 (FRALOG(6)=FRALOQ(6)=1)	1.03 ± 0.01
Cojets612 (FRALOG(6)=FRALOQ(6)=2)	1.04 ± 0.01

Table 6: Values of the asymmetry ratio R from Jetset, with perfect gluon jet identification and including simulation of the detector, for $d\bar{d}$ events and $b\bar{b}$ events. The errors are statistical only.

Region	$d\bar{d}$ events	$b\bar{b}$ events
(1)	1.64 ± 0.10	1.48 ± 0.09
(2)	1.77 ± 0.18	1.99 ± 0.19
(3)	1.95 ± 0.16	1.72 ± 0.13
(4)	2.15 ± 0.17	2.11 ± 0.16
(5)	1.50 ± 0.12	1.30 ± 0.12
(6)	1.63 ± 0.15	1.80 ± 0.18

Figure Captions

Figure 1. (a) A 3-jet event in e^+e^- annihilations. In the Lund string model for fragmentation, string segments span the region between the quark q and gluon g and between the antiquark $\overline{q}$ and gluon, as shown by the dotted lines. (b) A 3-jet event with the gluon and antiquark jet directions and energies transposed relative to the event of (a).

Figure 2. Particle flow distributions $(1/N)\, dn/d\psi$ for event configurations (I) and (II). No corrections have been applied to the data. The points with errors show the flow from the high energy quark jet to the low energy quark jet then to the gluon jet; the histogram shows the measured particle flow for the same events, again starting at the high energy quark jet but then proceeding in the opposite sense. The dashed lines show the regions used for calculation of the asymmetry ratios R.

Figure 3. Particle flow distributions $(1/N)\, dn/d\psi$ for event configurations (III) and (IV). No corrections have been applied to the data. The points with errors show the flow from the high energy quark jet to the low energy quark jet then to the gluon jet, for samples (IIIa) and (IVa); the histogram shows the flow from the high energy quark jet to the gluon jet then to the low energy quark jet, for samples (IIIb) and (IVb). The dashed lines show the regions used for calculation of the asymmetry ratios R.

Figure 1

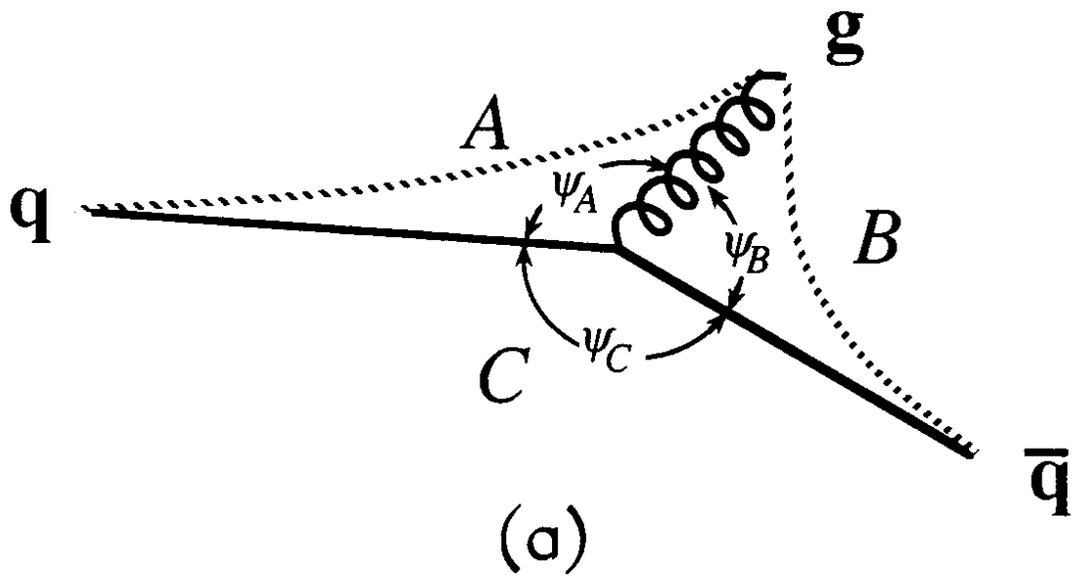

(a)

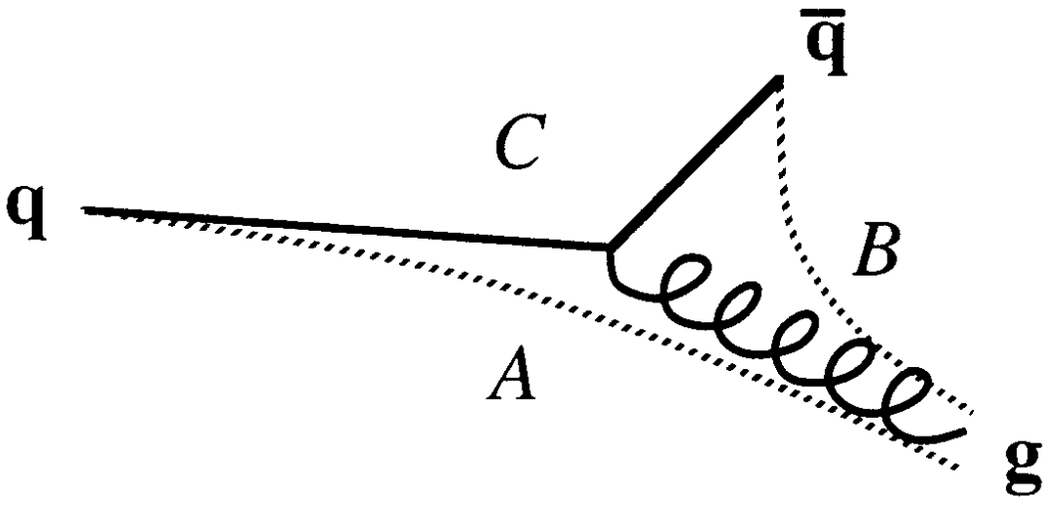

(b)

Figure 2

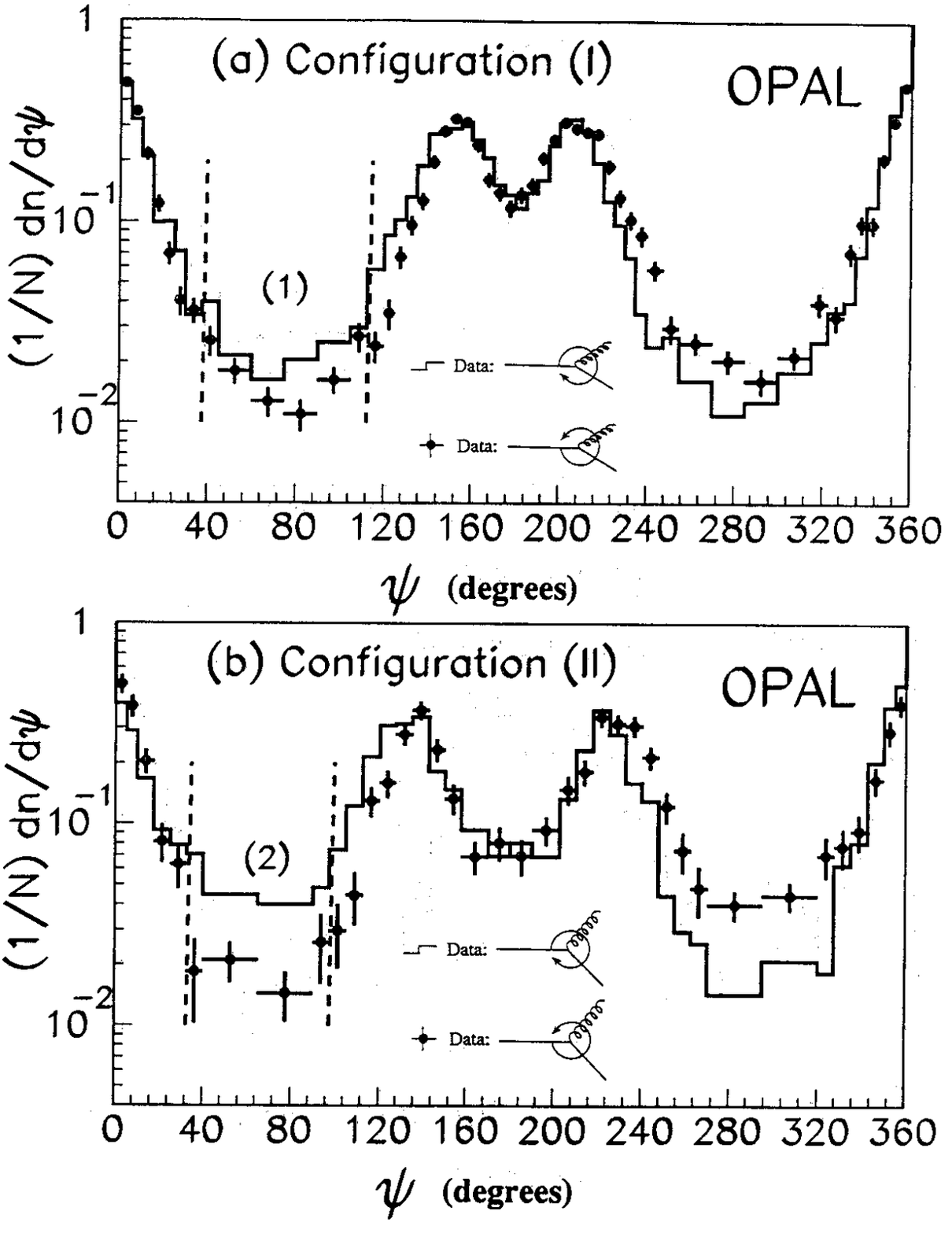
(a) Configuration (I)
OPAL
(1)
Data:
Data:
(1/N) dn/dψ
1
10⁻¹
10⁻²
0 40 80 120 160 200 240 280 320 360
ψ (degrees)
(b) Configuration (II)
OPAL
(2)
Data:
Data:
(1/N) dn/dψ
1
10⁻¹
10⁻²
0 40 80 120 160 200 240 280 320 360
ψ (degrees)

Figure 3

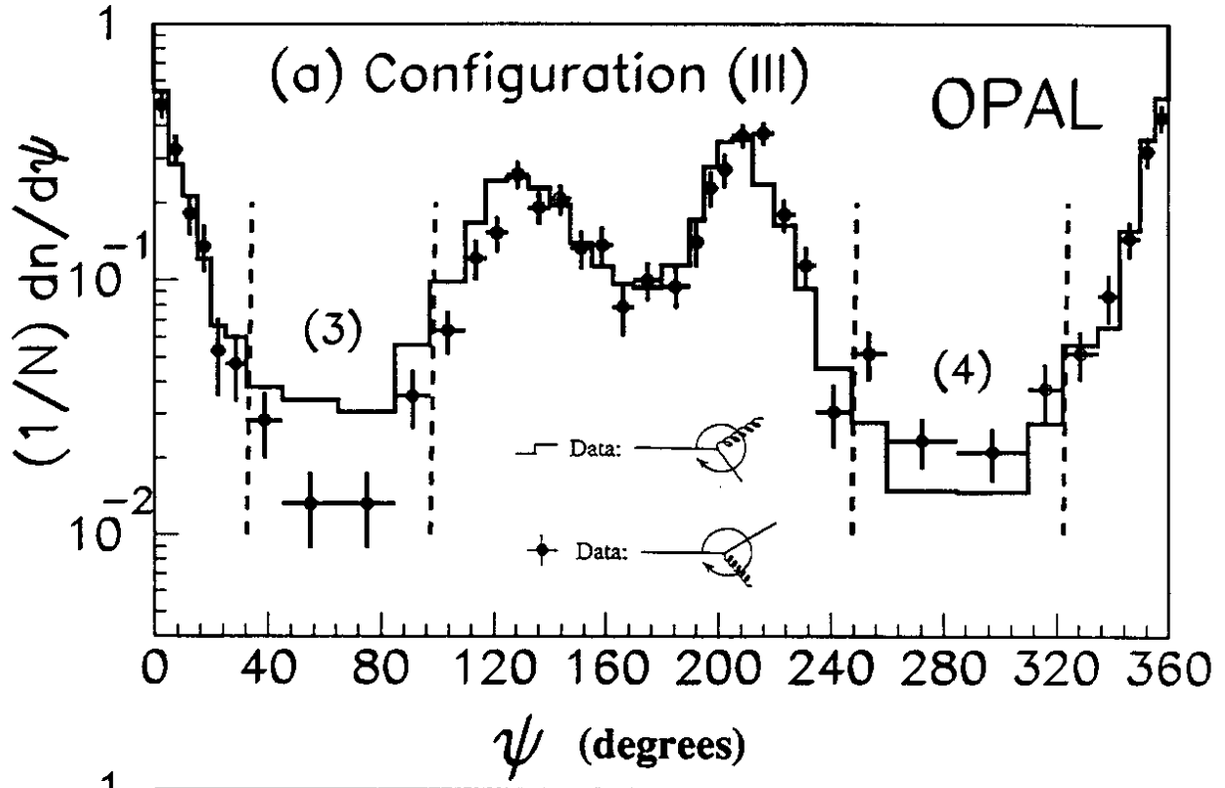

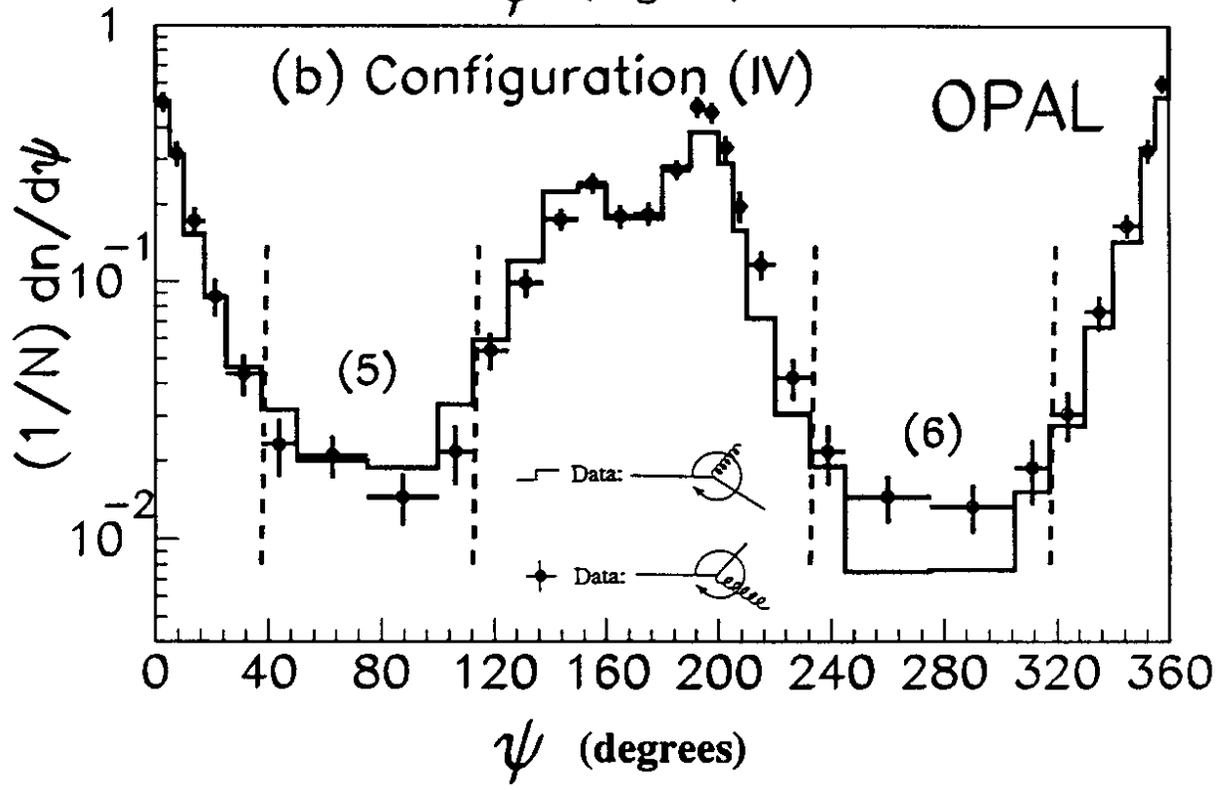

Imprimé au CERN. Prix : 0.70 Fr.